RSC Advances

ROYAL SOCIETY OF CHEMISTRY

www.rsc.org/advances

Table of Contents Entry

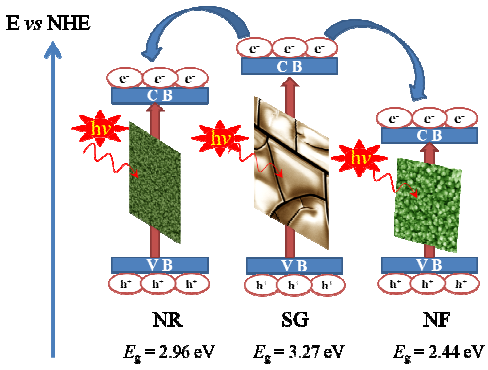

Appropriate layer-by-layer alignment of titania thin films with one/three- dimensional nanostructures achieved an enhanced photocatalytic activity.

Sandwich-like Titania Thin Films with One/Three- Dimensional Nanostructures for Photocatalytic Applications

Ming-Zao Tang[a] and Jin-Ming Wu[*a]

This study attempts to construct a multi-layer titania with merits inherent from both one/three- dimensional nanostructures and phase junctions. A solution-based technique was adopted to fabricate a sandwich-like titania thin film with one/three- dimensional nanostructures. The film consisted of one-dimensional anatase/rutile nanorod arrays as the underlayer and three-dimensional rutile nanoflower arrays as the top layer, which were intercalated with a sol-gel anatase nanoparticulate layer. The surface morphology, phase composition and light absorption behavior were characterized in detail by field emission scanning electron microscope (FE-SEM), X-ray diffraction (XRD) pattern and UV-vis diffuse reflectance spectra (UV-vis DRS). When utilized to assist photodegradation of rhodamine B in water, the sandwich film possessed an efficiency significantly higher than the sum of those derived by three component films. The appropriate layer-by-layer alignment of nanostructured films is thus argued to be a feasible route to fabricate titania thin films with high photocatalytic actives.

I. Introduction

Titania (TiO_2) has found wide applications in gas sensors,[1] photocatalysis,[2] photoelectrocatalysis[3] and photovoltaics.[4] However, a high electron-hole recombination rate or low photogenerated charge transfer rate restricts the efficiency of photon-induced procedures, thus limited its practical applications in energy conversion and environment remediation. When utilized as photocatalysts to achieve water splitting or photodegradation of organic pollutants, improved charge separation rate and hence enhanced photocatalytic activity can be realized through the various strategies of noble-metal deposition,[5] metal doping,[6] non-metal doping,[7] surface sensitizing,[8] semiconductor-coupling,[9] and more recently, graphene-coupling.[10] Alternatively, many efforts have also been made to fabricate titania with different one/three- dimensional nanostructures including but not limited to nanotubes,[11] nanorods,[12] nanoflowers,[13] nanowires,[14] whiskers,[15] needles[16] and sheets/plates.[17] Such titania nanostructures with extremely high specific surface area not only provide high density active sites for photochemical reactions, but also accelerate significantly the transfer rate of photoelectrons, which hence inhibits the recombination of photogenerated holes and electrons and in turn improves the photocatalytic activity.

The commercial available Degussa P25 nanoparticles, which consist of 80% anatase and 20% rutile, exhibit high activity for several photocatalytic reactions. The high efficiency has been believed to result from a synergetic effect arising from the anatase and rutile particles that are in contact.[18] Several junctions of anatase/rutile,[19] anatase/brookite,[20] and anatase/TiO_2-B[21] have been reported, which contribute to the photo-induced property as a result of the matching band potential. In our group, a composite titania thin film consisted of quasi-aligned single-crystalline rutile nanorods embedded in sol-gel anatase aggregates has been constructed.[22] The combination of the two components significantly improved the charge separation rate because the single-crystalline rutile nanorods provided channels for a rapid transfer of electrons that photogenerated on the anatase/rutile junction. The synergetic effect was also identified on a dual-layer titania film consisted of a sol-gel anatase layer over an interconnected porous anatase one.[23]

Based on the numerous literatures reporting the positive effects of either one/three- dimensional nanostructures[10-16] or phase coupling[17-22] for titania, it is reasonable to combine the two effective tactics to achieve a novel titania thin film with high photocatalytic activity. Herein, we report a novel sandwich-like titania thin film in which the components are all titania, but with different crystal structures and nanofeatures. The unique structure and phase composition were found to significantly favor the effective utilization of UV light during photodegradation of rhodamine B in water. The current study thus evidenced the possibility of achieving high efficiency titania thin films via an appropriate layer-by-layer alignment of titania thin films with one/three- dimensional nanostructures.

II. Experimental Procedure

2.1 Fabrications of titania sandwich films

2.1.1 Preparation of titania nanorod underlayer

Titanium plates of the dimensions $5 \times 5 \times 0.01$ cm^3 were etched at ambient temperature in a 1:3:6 (in volume) mixture of a 55 mass% HF aqueous solution, a 63 mass % HNO_3 aqueous solution and distilled water for 30 seconds to remove the naturally formed surface oxides, followed by cleaning with distilled water in an ultrasonic bath for 20 min. Each of such pickled Ti plates was immersed in a 50 ml 30 mass% H_2O_2 solution and kept for 72 h in an oven maintained at 80 ^oC.[12a] The surface oxidized titanium plates (named **NR** hereafter) were then rinsed gently in distilled water and dried for the subsequent sol-gel dip-coating.

2.1.2 Coating of sol-gel intermediate layer

Titania sol was prepared as follows:[24] 4.25 mL of titanium (IV) butoxide and 1.2 mL of diethanolamine were dissolved in 14.3 mL of ethanol. The mixture was stirred vigorously for 2 h at ambient temperature, followed by slowly adding a solution of 0.25 mL of distilled water and 2.5 mL of ethanol. A further stir of the mixture was conducted for 3 h to form the sol. The NR substrate was dipped into the sol for 1 min and then lifted out of the sol at a speed of 6 mm/s under a relative humidity of ca. 15%. The procedure was repeated three times to get a sol-gel layer with a thickness of ca. 0.5 μm. The film (named **NR/SG** hereafter) was then dried at 105 ^oC for 1 h. The same procedure was applied to the metallic Ti substrate to prepare the sample **SG**.

2.1.3 Deposition of titania nanoflower top layer

To prepare the precursor solution, as-pickled Ti plates were immersed in a 50 ml 30 mass% H_2O_2 solution which contained 1.0 ml concentrated nitric acid and 100 mg hexamethylenetetramine (HMT), and kept in an oven maintained at 80 °C for 48 h. The Ti plate was then taken out and the achieved solution was subjected to centrifugation at a rotation speed of 3000 rpm for 5 min to remove the suspensions. Several parallel reactions were carried out to collect enough amounts of the precursor solution, which contained ca. 4.8 mM hydrated Ti (IV) ions and ca. 0.66 M nitrate ions with a pH value of ca. 0.6.[25]

The NR/SG samples were immersed into 15 mL of the precursor solution achieved above, together with 500 mg sponge titanium, and maintained at 80 ^oC for 24 h. After the deposition, the sample was taken out, rinsed with distilled water and followed by a final heat treatment conducted at 450 ^oC for 1 h in air. Such titania sandwich films are designated as **NR/SG/NF**

hereafter for simplicity. The precipitation procedure was also adopted on substrates of metallic Ti and sol-gel layer (SG), respectively, to achieve the sample **NF** and **SG/NF**. All the titania films mentioned in the text are subjected to a final calcination in air at 450 ^{o}C for 1 h before characterizations.

2.2 Film characterization

The surface morphology was examined using a field emission scanning electron microscope (FE-SEM, S-4800, Hitachi, Japan). The X-ray diffraction (XRD) measurements were conducted on a Rigaku D/max-3B diffractometer with CuK_{α} radiation, operated at 40 kV, 36 mA (λ = 0.154056 nm). UV-vis diffuse reflectance spectra of titania films were collected using a UV-vis near-infrared spectrometer (UV-3150, Shimadzu, Japan). The X-ray photoelectron spectra (XPS) characterization was carried out on an Escalab 250Xi system (Thermo Fisher Scientific). The binding energy was calibrated by using the surface containment carbon (C 1s = 284.6 eV).

2.3 Photocatalytic activity evaluations

The photocatalytic activity was evaluated using rhodamine B (RhB) aqueous solution as the probe in a pyrex reactor with a water jacket. A 50 mL sample of RhB with an initial concentration of 0.005 mM in the presence of the samples (2.5 × 2.5 cm^2) was illuminated with a 18 W ultraviolet lamp 6 cm above the solution. The average intensity of UV irradiance reaching the samples was measured to be ca. 4.5 mW/cm^2, using an irradiance meter (Model: UV-A, Beijing Normal University, China, measured for the wavelength range of 320 - 400 nm with a peak wavelength of 365 nm). During the reaction, the solution was stirred continuously and exposed to air. The change in RhB concentration was monitored with a UV-vis spectrophotometer (UV-1800PC, Shanghai Mapada Instruments Co. Ltd, Shanghai, China) at a wavelength of 555 nm, using a quartz cuvette of 10 mm of the optical path length.

III. Results and discussion

Figure 1 shows the FE-SEM morphology of the titania nanorod film NR, that covered with a sol-gel anatase layer NR/SG, and the sandwich film NR/SG/NF. The titania nanorods, with the size of ca. 200 nm in length and ca. 30 nm in diameter, grew vertically upside from the Ti substrate, forming a titania nanorod array (Figure 1a) with a film thickness of ca. 1 μm. After the dip-coating procedure, the nanorods were covered completely by the sol-gel anatase, which was full of cracks (Figure 1b). For the sandwich film, the flower-like aggregates precipitated on the sol-gel layer and covered thoroughly the whole surface. The homogeneous film on the top consisted of titania nanoflowers formed by self-assembled nanorods with an average size of ca. 70 nm in diameter and 150 nm in length (Figure 1c). Figure 1d illustrates a cross-sectional observation recorded from a naturally occurred crack. The film thickness of the top nanoflowers layer and the intermediate sol-gel layer was estimated to be similar of 0.5 μm. The nanorod layer possessed a total film thickness of 3 μm, including a 2μm-thick anatase nanoparticulate layer between the nanorod array and the Ti substrate.[26] The film thickness of the sandwich film is thus estimated to be ca. 4 μm.

Figure 2 shows the XRD patterns of the corresponding titania films. It could be identified from the patterns that the rod-like underlayer array NR consisted of a mixture of well-crystallized anatase and rutile. The sol-gel-derived titania middle layer mainly consists of phase pure anatase,[22] which increased slightly the intensity of XRD peaks corresponding to anatase of the sample NR/SG. After the flower-like top layer was precipitated onto the sample to form sandwich films NR/SG/NF, the intensity of XRD peaks corresponding to rutile increased significantly, especially the strong peak located at 2θ=36.08^{o} which corresponds to the (101) plane of rutile titania according to JCPDS card 21-1276, suggesting that the nanoflower top layer mainly consisted of oriental rutile titania grown along the (101) plane.

Figure 3a demonstrates the UV-vis diffuse reflectance spectra collected from the various titania films of NR, NR/SG, and NR/SG/NF. The sandwich film exhibited lower reflectance in UV light region when compared with NR and NR/SG, especially in the wavelength region between 320 nm to 400 nm. This suggests that the sandwich film has a much better capability in absorbing UV light, thus increasing the efficiency for light energy utilization. Assuming an indirect transition between bands for titania, Figure 3b shows the re-plotting of absorption as a function of wavelength in the $\alpha^{1/2} \sim h\nu$ coordinate to evaluate the corresponding band gap (E_g) of titania films, where α is the absorption coefficient and $h\nu$ is the photon energy.[27] This figure illustrates that the present three titania films possessed similar indirect band gap of 2.94~2.96 eV.

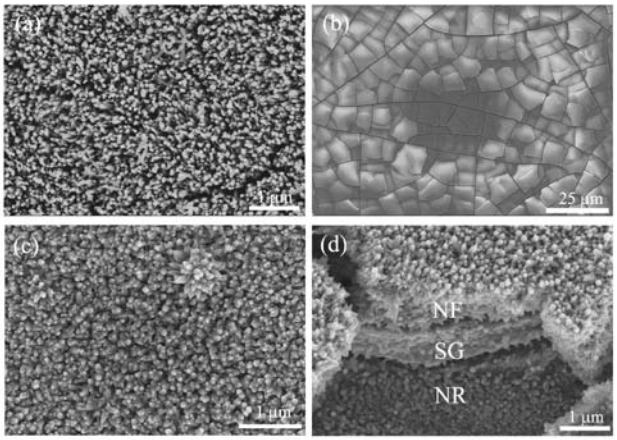

Fig. 1 FE-SEM morphologies of (a) the nanorod thin film (NR), (b) that after sol-gel dip-coating of anatase layer (NR/SG), and (c, d) followed by a subsequent precipitation of rutile nanoflowers (NR/SG/NF).

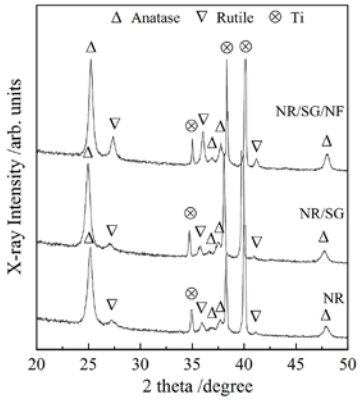

Fig. 2 XRD patterns of the nanorod thin film (NR), that after sol-gel dip-coating of anatase layer (NR/SG), and followed by a subsequent precipitation of rutile nanoflowers (NR/SG/NF).

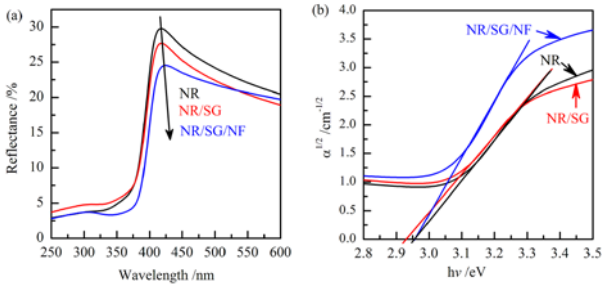

Fig. 3 (a) UV-vis diffuse reflectance spectra of the nanorod thin film (NR), that after sol-gel dip-coating of anatase layer (NR/SG), and followed by a subsequent precipitation of rutile nanoflowers (NR/SG/NF). (b) Re-plotting of (a) in the $\alpha^{1/2} \sim h\nu$ coordinate to evaluate the corresponding band gap, assuming an indirect transition between bands for titania.

Table 1 Film thickness, band gap, grain size, weight percentage of anatase w_A for the various titania films, the reaction rate constant k and correlation coefficient R when utilized to assist photodegradation of rhodamine B in water.

Titania film	Film thickness /μm	Band gap (E_g) /eV	Grain size /nm		w_A /%	k /$\times 10^{-3}$ min^{-1}	R
			Anatase	Rutile			
NR	3.0	2.96	15	27	67	3.9	0.975
SG	0.5	3.27[§]	25[§]	—	100[§]	0.3	0.905
NF	0.5	2.44[¶]	—	17[¶]	0	4.7	0.980
NR/SG	3.5	2.94	17	27	93	0.9	0.936
SG/NF	1.0	2.53[#]	—	36[#]	0[#]	4.8	0.974
NR/SG/NF	4.0	2.96	20	33	79	12.3	0.994

[§] Data derived from Ref. [23]; [¶] Data derived from Ref. [31]; [#] Refer to online ESI for the original UV-Vis diffuse reflectance spectrum (Figure S1) and XRD pattern (Figure S2) utilized to estimate the data listed. It's noted that no peaks arising from the sol-gel anatase under layer were detected, which can be attributed to the limited film thickness.

Table 1 summarizes the band gap for the various titania films, together with other key parameters affecting readily the photocatalytic activity, which include film thickness, grain size, and weight percentage of anatase. Here, the band gap was estimated from the UV-Vis diffuse reflectance spectra, and the grain size and phase composition were calculated from the XRD patterns (see Electronic Supplementary Information, ESI,[†] for details). The band gap of sol-gel anatase (3.27 eV) is near to that of bulk anatase; yet much lower band gaps of 2.44 eV and 2.53 eV were measured for the rutile nanoflower layers precipitated on metallic Ti and sol-gel anatase layer, respectively, both of which are far smaller than that of bulk rutile (3.0 eV). The sandwich film consisted of 79 wt. % anatase and 21 wt. % rutile in phase composition, which is near to P25 titania nanoparticles.[18] When compared with that precipitated on metallic Ti substrates, the rutile nanoflowers precipitated on the sol-gel layer possessed a larger grain size. As a result, a larger rutile grain size was estimated for the sample NR/SG/NF when compared with the sample NR and NR/SG.

Figure 4 illustrates the XPS spectra of the O 1s and N 1s core levels collected from the various titania films of NR, SG, and NF. The O 1s spectra are similar (Fig. 4a), suggesting that the much lower band gap of NF when compared with that of NR and SG cannot be attributed to the possible oxygen-deficiencies in titania.[28] A remarkable peak located at ca. 400 eV, which corresponds to interstitial nitrogen or surface-bound ammonia,[29] can be discerned only in the film NF. This indicates that the much lower band gap of rutile nanoflowers precipitated on both metallic Ti (NF) and sol-gel anatase layer (SG/NF) may result from the interstitial nitrogen doping,[29] which resulted from the decomposition of HMT in the precursor solution. The band gap of NR/SG/NF was not lowered significantly by the top NF layer because the underlayer NR comprised 7/8 in thickness of the total composite film.

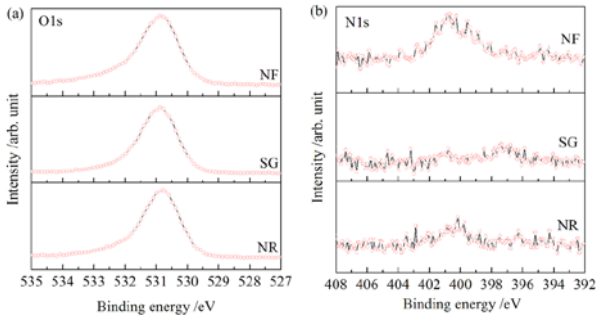

Fig. 4 XPS spectra of (a) O 1s and (b) N 1s core levels of the various titania thin films on metallic Ti substrates. NR: titania nanorod array; SG: sol-gel dip-coated anatase; NF: rutile nanoflower array.

Figure 5a indicates typical photodegradation curves of RhB in water in the presence of NR, NR/SG, and NR/SG/NF. Under the irradiation of the UV lamp, the decomposition of RhB is ignorable in absence of titania.[26] For RhB aqueous solution with a dilute initial concentration, the photodegradation reaction follows roughly a pseudo-first order reaction,[30]

$$c = c_0 \exp(-kt) \quad (1)$$

where c_0 and c are the initial concentration and that after the reaction duration t, respectively, and k is the pseudo-first order reaction rate constant. Re-plotting the data in the $\ln(c_0/c) \sim t$ scale (shown in Figure 5b) gave k values of 3.9×10^{-3}, 0.3×10^{-3} and 12.3×10^{-3} min^{-1}, corresponding to the NR, NR/SG and NR/SR/NF samples, respectively. It could be found that the photocatalytic activity of the titania sandwich films NR/SG/NF was 3.2 times that of NR, 41 times that of SG, and 2.6 times that of NF (Table 1). When compared with the sum of the reaction rate constants derived from three component films of NR, SG and NF, an extra improvement of ca. 38% can also be discerned for the sandwich film NR/SG/NF. When considering the large grain size (Table 1), this fact suggests clearly a synergetic effect arising from the layer-by-layer alignments.

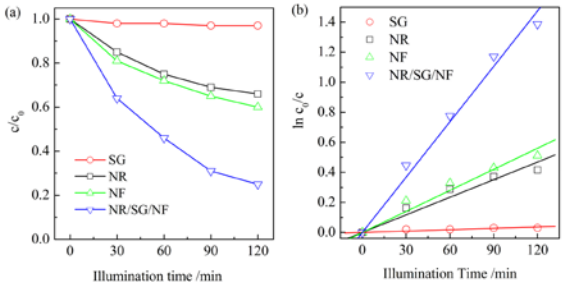

Fig. 5 (a) Photodegradation curves and (b) pseudo-first order reaction fitting results for the degradation of rhodamine B in water in the presence of various titania films as listed in Table 1.

It can be discerned from Table 1 that the top layer that exposed directly to the target solution determines to the great extent the efficiency. In the current investigation, the sol-gel layer exhibited the lowest activity to assist photodegradation of RhB in water. The composite of NR and SG with SG as top layer (NR/SG) resulted in an efficiency slightly higher than that of SG, yet remarkably lower than that of NR. The composite of NF on top of SG (SG/NF) achieved a further enhancement in photocatalytic activity when compared with that of NF.

Titania thin films with one/three- dimensional nanofeatures have been reported to exhibit advantageous photocatalytic activity over that consisted of zero-dimensional nanoparticles.[11-17,30] The present study suggests that, titania thin

films with even higher photocatalytic activity can be achieved by appropriate configurations of high efficiency titania films with distinct morphology and phase compositions. As for the present sandwich film, the enhanced photocatalytic activity should firstly be contributed to the top layer with unique nanofeature of nanoflowers, which are aggregates of well-crystallized single-crystalline rutile nanorods.[22,31] The unique nanoflower layer not only possessed high specific surface area, which favors adsorption of target molecules and provides more active sites for the photodegradation reaction, but also enhanced charge separation rate, which resulted from the well-crystallized single-crystalline nanorods[31]. In addition, the gaps among the nanoflowers in the top layer and the cracks on the intermediate sol-gel layer allow the inner diffusion of target molecules to three component layers, and at the same time the outer diffusion of photogenerated active species from three component layers to the target solution. Therefore, one can expect that the well-established band gap matching mechanism[19-21] favoring the charge separation, as illustrated schematically in Figure 6, also functions in the sandwich film. The band gap for titania is 3.2 eV in anatase and 3.0 eV in rutile. Also, it is generally accepted that the conduction band of anatase lies 0.2 eV above that of rutile.[32] Upon the UV light illumination, photogenerated electrons from the intermediate sol-gel anatase layer migrate to the neighboring rutile nanorods on either bottom layer or top layer, which improves significantly its contributions to the photocatalytic activity of the sandwich film. For the dual composite films of NR/SG and SG/NF, such an improvement is not so remarkable; however, for the sandwich film of NR/SG/NF, the enhancement in photocatalytic activity arising from the band gap match is more significant. This can be partly explained by the enhanced absorption of UV light for the sandwich film as illustrated in Figure 3.

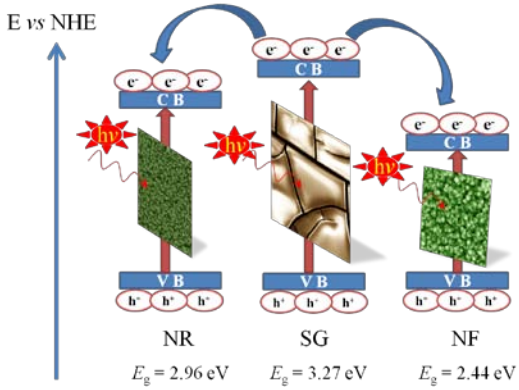

Fig. 6 A schematic image explaining the improved photocatalytic activity of the sandwich film resulting from the enhanced charge separation of the sol-gel anatase intermediate layer.

A recent study by Scanlon et al. suggested a different band alignment of rutile and anatase TiO_2, in which the migration direction of the photogenerated charge carriers was opposite to that indicated in Fig. 6.[33] However, this will not affect the charge separation effect arising from the phase junction.

It can be anticipated that appropriate optimizations in photocatalytic activity for each component films, utilizing well-established techniques such as doping, [6,7,34] sensitizing,[8,35] noble metals deposition,[5] should help successful constructions of sandwich titania films with excellent photocatalytic performances. The present study may thus give hints to research and development of high efficiency titania films for green energy and environment remediation.

IV. Conclusions

A titania sandwich film was successfully fabricated through a solution-based layer-by-layer route. A rod-like thin film containing both anatase and rutile titania was firstly fabricated on a metallic Ti substrate by direct oxidation in an aqueous H_2O_2 solution at 80 ^oC for 72 h, which was then covered by a sol-gel anatase layer, and further deposited by a flower-like rutile titania layer to achieve finally the sandwich films. The sandwich film consisted of 79% anatase and 21% rutile in weight percentage, and possessed a band gap of ca. 3.0 eV. Under a UV light illumination, the sol-gel layer, nanorod layer, and nanoflower layer exhibited a reaction rate constant of 0.3×10^{-3}, 3.9×10^{-3} and 4.7×10^{-3} min^{-1} for photodegradation of rhodamine B in water, respectively. Interestingly, the sandwich film exhibited a remarkable high reaction rate constant of 12.3×10^{-3} min^{-1}, which thus suggests a synergetic effect arising from the appropriate alignment of three component layers.

Acknowledgment

This work is supported by the Natural Science Foundation of Zhejiang Province, China (Project No. Y13E020001).

Notes and references

[a] *State Key Laboratory of Silicon Materials, Key Laboratory of Advanced Materials and Applications for Batteries of Zhejiang Province and Department of Materials Science and Engineering, Zhejiang University, Hangzhou 310027, P. R. China. Tel/Fax: +86-571-87953115, E-mail: msewjm@zju.edu.cn*

† Electronic Supplementary Information (ESI) available: Equations for calculating the average grain size d_{hkl} and the fraction of anatase w_A as listed in Table 1; UV-vis diffuse reflectance spectra and XRD patterns of rutile nanoflowers precipitated on sol-gel anatase layer (SG/NF).

1. O. K. Varghese, D. W. Gong, M. Paulose, K. G. Ong, E. C. Dickey and C. A. Grimes, *Adv. Mater.*, 2003, **15**, 624.
2. X. B. Chen and S. S. Mao, *Chem. Rev.*, 2007, **107**, 2891.
3. M. Antoniadou, V. M. Daskalaki, N. Balis, D. I. Kondarides, C. Kordulis and P Lianos, *Appl. Catal. B*, 2006, **151**, 3399.
4. H. An, D. Song, J. Lee, E. M. Kang, J. Jaworski, J. M. Kim and Y. S. Kang, *J. Mater. Chem. A*, 2014, **2**, 2250.
5. (a) A. A. Ismail, D. W. Bahnemann, J. Rathousky, V. Yarovyi and M. Wark, *J. Mater. Chem.*, 2011, **21**, 7802; (b) M. V. Dozzi, A. Saccomanni, M. Altomare and E. Selli, *Photochem. Photobiol. Sci.*, 2013, **12**, 595.
6. W. Y. Choi, A. Termin, M. R. Hoffmann, *J.Phys. Chem.*, 1994, **98**, 13669.
7. L. G. Devi and R. Kavitha, *Appl. Catal. B: Environ.*, 2013, **140-141**, 559.
8. Z. Wang, C. Chen, W. Ma and J. Zhao, Sensitization of titania semiconductor: a promising strategy to utilize visible light, in: Photocatalysis and Water Purification: From Fundamentals to Recent Applications, Ed. P. Pichat, Wiley-VCH Verlag GmbH & Co. KGaA, Weinheim, Germany, 2013, 199-240.
9. X. M. Song, J. M. Wu and M. Yan, *Electrochem. Commun.*, **2009**, 11, 2203.
10. Q. Xiang, J. Yu and M. Jaroniec, *Chem. Soc. Rev.*, 2012, **41**, 782.
11. (a) L. B. Fen, T. K. Han, N. M. Nee, B. C. Ang and M. R. Johan, *Appl. Surf. Sci.*, 2011, **258**, 431; (b) S. Kim, M. Kim, S. H. Hwang and S. K. Lim, *Appl. Catal. B*, 2012, **123**, 391; (c) A. Hazra, B. Bhowmik, K. Dutta, V. Manjuladevi, R. K. Gupta, P. P. Chattopadhyay and P. Bhattacharyya, *Sci. Adv. Mater.*, 2014, **6**, 714.
12. (a) J. M. Wu, *J. Cryst. Growth*, 2004, **269**, 347; (b) H. G. Yu, J. G. Yu, B. Cheng and J. Lin, *J. Hazard. Mater.*, 2007, **147**, 587.
13. (a) J. M. Wu and B. Qi, *J. Phys. Chem.* C, 2007, **111**, 666; (b)

A. Arun, D. K. Chacko, A. A. Madhavan, T. G. Deepak, G. S. Anjusree, T. Sara, S. Ramakrishna, S. V. Nair and A. S. Nair, *RSC Adv.*, 2014, **4**, 1421; (c) Z. Wu, Q. Wu, L. Du, C. Jiang and L. Piao, *Particuology*, 2013, http://dx.doi.org/10.1016/j.partic.2013.04.003.

14. (a) J. M. Wu and H. X. Xue, *J. Am. Ceram. Soc*. 2009, **92**, 2139; (b) F. Amano, T. Yasumoto, T. Shibayama, S. Uchida and B. Ohtani, *Appl. Catal. B*, 2009, **89**, 583; (c) B. Li, J. M. Wu, T. T. Guo, M. Z. Tang and W. Wen, *Nanoscale*, 2014, **6**, 3046.
15. A. Vuorema, J. J. Walsh, M. Sillanpää, W. Thielemans, R. J. Forster and F. Marken, *Electrochim. Acta*, 2012, **73**, 31.
16. P. Cheng, J. Qiu, M. Gu, Y. Jin and W. Shangguan, *Mater. Lett*., 2004, **58**, 3751.
17. (a) W. Wang, Y. R. Ni, C. H. Lu and Z. Z. Xu, *RSC Adv.*, 2012, **2**, 8286; (b) M. J. Xu, F. Teng, J. Xu, T. Y. Lu and M. D. Chen, *RSC Adv.*, 2014, **4**, 8023; (c) G. Kim, C. Jo, W. Kim, J. Chun, S. Yoon, J. Lee and W. Choi, *Energy Environ. Sci.*, 2013, **6**, 2932.
18. (a) R. I. Bickley, T. Gonzalez-Carreno, J. S. Lees, L. Palmisano and R. J. D. J. Tilley, *Solid State Chem.*, 1991, **92**, 178; (b) T. Ohno, K. Sarukawa, K. Tokieda and M. Matsumura, *J. Catal.*, 2001. **203**, 82; (c) B. Ohtani, O. O. Prieto-Mahaney, D. Li and R. Abe, *J. Photochem. Photobiol. A*, 2010, **216**, 179.
19. (a) Q. Xu, Y. Ma, J. Zhang, X. Wang, Z. Feng and C. Li, *J. Catal.*, 2011, **278**, 329; (b) D. O. Scanlon, C. W. Dunnill, J. Buckeridge, S. A. Shevlin, A. J. Logsdail, S. M. Woodley, C. R. A. Catlow, M. J. Powell, R. G. Palgrave, I. P. Parkin, G. W. Watson, T. W. Keal, P. Sherwood, A. Walsh and A. A. Sokol, *Nat. Mater.*, 2013, **12**, 798; (c) Y. X. Liu, Z. L. Wang, W. D. Wang and W. X. Huang, *J. Catal.*, 2014, **310**, 16.
20. (a) T. Ozawa, M. Iwasaki, H. Tada, T. Akita, K. Tanaka and S. Ito, *J. Colloid Interf. Sci.*, 2005, **281**, 510; (b) S. Ardizzone, C. L. Bianchi, G. Cappeletti, S. Gialanella, C. Pirola and V. Ragaini, *J. Phys. Chem. C*, 2007, **111**, 13222; (c) X. J. Shen, J. L. Zhang, B. Z. Tian and M. Anpo, *J. Mater. Sci.*, 2012, **47**, 5743.
21. (a) W. Li, C. Liu, Y. X. Zhou, Y. Bai, X. Feng, Z. H. Yang, L. H. Lu, X. H. Lu and K. Y. Chan, *J. Phys. Chem. C*, 2008, **112**, 20539; (b) J. Jitputti, Y. Suzuki and S. Yoshikawa, *Catal. Commun.*, 2008, **9**, 1265; (c) H. H. Lo, N. O. Gopal, S. C. Sheu and S. C. Ke, *J. Phys. Chem. C*, 2014, **118**, 2877.
22. X. M. Song, J. M. Wu, M. Z. Tang, B. Qi and M. Yan, *J. Phys. Chem. C*, 2008, **112**, 19484.
23. X. M. Song, J. M. Wu, G. J. Zhang and M. Yan, *J. Phys. Chem. C*, 2009, **113**, 10681.
24. J. Yu, X. Zhao, J. Du and W. Chen, *J. Sol-Gel. Sci. Technol.*, 2000, **17**, 163.
25. J. M. Wu and B. Qi, *J. Am. Ceram. Soc.*, 2008, **91**, 3961.
26. J. M. Wu, T. W. Zhang, Y. W. Zeng, H. Satoshi, K. Tsuru, and A. Osaka, *Langmuir*, 2005, **21**, 6995.
27. E. Sanchez and T. Lopez, *Mater. Lett.*, 1995, **25**, 271.
28. (a) U. Diebold, *Surf. Sci. Rep.*, 2003, **48**, 53; (b) J. Sun and J. M. Wu, *Sci. Adv. Mater.*, 2013, **5**, 549.
29. C. W. Dunnill and I. P. Parkin, *Chem. Vap. Depostion*, 2009, **15**, 171.
30. (a) J. M. Wu, *Environ. Sci. Technol.*, 2007, **41**, 1723; (b) Y. W. Wang, L. Z. Zhang, K. J. Deng, X. Y. Chen and Z. G. Zou, *J. Phys. Chem. C*, 2007, **111**, 2709**.**
31. M. Z. Tang and J. M. Wu, *Sci. Adv. Mater*., 2009, **1**, 144.
32. L. Kavan, M. Grätzel, S. E. Gilbert, C. Klemenz and H. J. Scheel, *J. Am. Chem. Soc*, 1996, **118**, 6716**.**
33. D. O. Scanlon, C. W. Dunnill, J. Buckeridge, S. A. Shevlin, A. J. Logsdail, S. M. Woodley, C. R. A. Catlow, M. J. Powell, R. G. Palgrave, I. P. Parkin, G. W. Watson, T. W. Keal, P. Sherwood, A. Walsh and A. A. Sokol, *Nature Mater.*, 2013, **12**, 798.
34. (a) L. Rizzo, D. Sannino, V. Vaiano, O. Sacco, A. Scarpa and D. Pietrogiacomi, *Appl. Catal. B: Environ.*, 2014, **144**, 369; (b) Z. Wang, C. Y. Yang, T. Q. Lin, H. Yin, P. Chen, D. Y. Wan, F. F. Xu, F. Q. Huang, J. H. Lin, X. M. Xie and M. H. Jiang, *Adv. Funct. Mater.*, 2013, **23**, 5444.
35. (a) A. Kruth, A. Quade, V. Bruser and K. D. Weltmann, *J. Phys. Chem. C*, 2013, **117**, 3804; (b) W. Geng, H. Liu and X. Yao, *Phys. Chem. Chem. Phys.*, 2013, **15**, 6025.